Chapter 4

Super Twisting Sliding Mode Control with Region Boundary Scheme for an Autonomous Underwater Vehicle

Vina Wahyuni Eka Putranti and Zool Hilmi Ismail

Additional information is available at the end of the chapter

http://dx.doi.org/10.5772/67579

Abstract

A robust tracking control for an Autonomous Underwater Vehicle (AUV) system operated in the extreme ocean environment activities is very much needed due to its external disturbances potentially disturb the stability of the system. This research proposes a new robust-region based controller which integrates Super Twisting Sliding Mode Control (STSMC) with region boundary approach in the presence of determined disturbances. STSMC is a second order SMC which combines between continuous signal and discontinuous signal to produce a robust system. By incorporating region based control into STSMC, the desired trajectory defined as a region produces an energy saving control compared to conventional point based control. Energy function of region error is applied on the AUV to maintain inside the desired region during tracking mission, thus, minimizing the energy usage. Analysis on a Lyapunov candidate proved that the proposed control achieved a global asymptotic stability and showed less chattering, providing 20s faster response time to handle perturbations, less transient of thrusters' propulsion and ability to save 50% of energy consumption compared to conventional SMC, Fuzzy SMC and STSMC. Overall, the newly developed controller contributed to a new robust, stable and energy saving controller for an AUV in the presence of external disturbances.

Keywords: super twisting sliding mode control, region boundary scheme, AUV

1. Introduction

An autonomous underwater vehicle (AUV) is employed with the aim to reduce the possibility of human accident in a long-term underwater mission. One of the important parts to be

installed on an AUV is an advance control system. Beside the capability to ensure the robustness and efficiency of an AUV, the selected control system must have the capability to minimize the effect of hazardous underwater environment such as sea current and hydrodynamics forces that potentially increase the energy usage since the position of AUV is moved from the desired trajectory. Various controllers are introduced to be adapted on the underwater vehicle. Linear quadratic regulator (LQR), linear quadratic Gaussian (LQG), H_2, and H_∞ are examples of optimal control used to design a method which optimize some desirable parameters. In Ref. [1], Joshi and Talange compared PID and linear quadratic regulator (LQR) to control the depth of REMUS 100 AUV. It was shown that the PID control took faster time response compared to LQR but it produced greater overshoot. The steady-state error was not produced by both controllers. Wadoo et al. proposed an optimal feedback control, H_2, for trajectory tracking case of kinematic model on an AUV [2]. In this chapter, H_2 was obtained by formulating LQG as a system of two-norm optimization problem. For the result, the proposed control showed an optimal design since it proved the robustness to the disturbances. However, the dynamics model of the AUV was not included. The types of AUV as well as the types of disturbances were also not mentioned.

Meanwhile, other researchers employed a sliding mode controller (SMC) which is robust against an inaccurate model and the external disturbances [3]. In this case, Cristi et al. designed the SMC from the Lyapunov candidate then applied it to adjust the AUV's maneuver based on the dynamics system and operating condition [4]. The simulation obtained a small error but it did not include the effect of the disturbances. The integrator SMC was also proposed by Hong et al. for the depth control of torpedo-shaped AUV in Ref. [5]. The SMC was applied as an inner pitch controller, while the effect of buoyancy on pitch and heave dynamics was considered. It was shown that the steady-state error existed and bounded within 0.15 m. Akcakaya et al. simulated the SMC based on the Lyapunov candidate to observe the yaw steering of the NPS AUV II model [6]. The effect of the disturbances was added in the simulation, and it was assumed that the AUV moved along x-axis with a constant speed of 0.75 ms^{-1}. The AUV completed the task even if disturbances were introduced. However, the chattering effect was produced in the switching condition when the system tried to reach the sliding surface of the SMC. This caused overconsumption of energy and could damage the AUV because the rudder changed rapidly [6].

Fuzzy logic control (FLC) is well known as an intelligent and adaptive control method [7]. For some cases, FLC is used to solve the chattering problem, thus, Guo et al. superposed SMC with fuzzy tuning technique [8]. Stability and robustness of the control system were guaranteed by selecting the shrinking and dilating factors of the fuzzy membership functions. Two experiments were conducted to observe the efficiency of the proposed controller for a Hai-Min underwater vehicle under the influence of ocean current. The results confirmed the effectiveness of the proposed scheme, although a poor transient performance was produced when the system tried to achieve precise tracking. At the transition moment, the state and sliding surface were separated by a significant distance. Lakehekar and Saundarmal developed an adaptive fuzzy sliding mode controller with a boundary layer scheme [9]. In the simulation, the SMC was required to manage the vertical position of the

http://dx.doi.org/10.5772/67579

AUV. However, the variables inside SMC changed dramatically. Thus, a boundary layer near the switching line was introduced as a new method. To maintain the states inside the layer, two fuzzy approximators were employed. The first approximator was used to update the slope's value in the sliding surface, while the second approximator was used to shape the error tracking. The result showed that the proposed controller reduced the reaching time of 1–2 s faster in overcoming the perturbations compared to the conventional SMC and the fuzzy SMC. However, better results were obtained after formulating good parameter conditions, which were produced by creating many rules. Moreover, the use of many rules increased the energy demand.

Neural network (NN) is commonly used either as a control plant model or as a controller [7, 10]. There are two kinds of learning processes in the NN, online learning and offline training, and the success of NN depends on selecting the correct learning process. Some cases reported that different responses could be resulted even after the same controller was applied under the same environment [11]. Ji-Hong et al. compared the conventional SMC with neural network (NN) SMC [12]. When the SMC is widely used as a robust control, NN is used in conjunction to minimize the nonlinearity of the dynamic's error [13]. The results show that the NN produced small errors and the AUV was able to track the trajectory after many learning and adaptation processes [14]. The effect of the disturbances was also not considered. Meanwhile, Van de ven et al. approximated the damping model of an AUV by using the value of velocity and acceleration under offline training process [10]. Noise was added in the second simulation, hence an online learning was adopted to decrease the state prediction error as well as to minimize the influence of the noise. It was shown that NN was used to improve the performance of poor identification of the AUV model. However, Van de ven et al assumed that other parts of the AUV model to be fully known, while in real case, the other parts such as added mass and also colioris and centripetal model were fully uncertain.

Another robust controller, which has been developed has a high order sliding mode controller (HOSMC), works on higher order derivatives of the sliding variable/system deviation [15–19]. The development of this method aimed to minimize the chattering effect produced by the conventional SMC. The second order is widely implemented because of the low information demand. Robust integral of sign of error (RISE) is included in the type of HOSMC. Fischer et al. used the RISE as a robust control of a six-DOF AUV [20]. The experimental setup was conducted in a swimming pool and an openwater sea trial with 0.08 ms^{-1} of flow current. It was shown that the RISE gave a good performance despite larger orientation error being produced in an openwater sea trial. Then, Fischer et al. superposed the RISE with NN to solve the issue of dynamics model error by using online learning technique [21]. The simulation result showed that the error converged 10 s faster under the proposed control. Experimental validation was the next plan for a further research. Rhif proposed second-order sliding mode control, named 2-SMC, to control the position and speed of a torpedo AUV [22]. The presence of external disturbances was considered in the simulation, although its value and type were not mentioned in detail. Chattering effect was reduced by proposed control. In Ref. [23], 2-SMC was applied to observe the stability of cyclops AUV under constant value of disturbances. The proposed control reduced the effect of disturbances and the steady-state error. For further

work, it was planned to develop the proposed control without decoupling some motions under sinusoidal disturbances.

Besides making a robust controller for the AUV, the other problem, which needs to be solved, was reducing the energy consumption. As stated in Ref. [6], the AUV could be damaged if it spends more energy. Li et al. was successful in introducing an adaptive region-tracking controller to overcome this weakness [24]. This success was followed by Ismail and Dunnigan [25]. The proposed controller in both the research guaranteed the error convergence of the sliding vector because the desired target was determined as a region instead of a point. The results showed that the thrusters were only activated when the AUV was outside the region. Therefore, the AUV reduced the energy consumption. Li and Cheah also used a similar approach for manipulator robot [26]. Li and Cheah proposed a unified objective bound method to merge the set point of the control, the trajectory tracking, and the performance bound. The desired trajectory reduced the conventional trajectory when the error was small, and it also changed to a dynamic region which could be scaled or rotated. Then, the system guaranteed the transient and the steady-state response of close loop system, as long as the objective was specified as a performance bound. A simulation was conducted to show the energy-saving properties of the proposed controller. The energy remained zero when the end effector of the arm robot started and stayed inside the bound. The proposed controller required less energy than the standard controller.

Reviewing from the advantages and the disadvantages of previous work, this chapter proposes a super twisting sliding mode control with region boundary for an AUV's tracking trajectory under the influence of perturbation. The proposed control is expected to obtain accuracy and efficiency, which is tracking precisely on the desired trajectory as well as saving energy consumption. The chapter is organized as follows: Section 2 studies about kinematic and dynamic model of a 6 DOF AUV, Section 3 describes the proposed control and comparison control, Section 4 performs results of simulation and analysis, while conclusion is explained in Section 5.

2. Kinematic and dynamic model

This section presents the kinematic and the dynamic model of a six-DOF AUV. Before discussing about the kinematic and the dynamic model, we introduce two types of geometric transformation in a six-DOF AUV, namely translation and rotations. The translation is represented by sway, surge, and heave movements, while the rotation is represented by roll, pitch, and yaw movements. An origin C, which is located on the center of the mass, a body-fixed reference and an earth-fixed reference, is used to describe the geometric transformation. The illustration can be seen in **Figure 1**.

The kinematic model studies about the relationship between inertial position of an AUV and velocity of an AUV. First, define the vector of position, vector of velocity, and vector of force as shown in Eq. (1) [27]:

http://dx.doi.org/10.5772/67579

$$\eta = [\eta_1;\ \eta_2]^T = [x,\ y,\ z;\ \phi,\ \theta,\ \psi]^T$$
$$v = [v_1;\ v_2]^T = [u,\ v, w;\ p,\ q,\ r]^T$$
$$\tau = [\tau_1;\ \tau_2]^T = [X,\ Y,\ Z; K,\ M,\ N]^T \quad (1)$$

where η indicates the linear and angular position, v indicates the linear and angular velocity, and τ indicates the linear and angular force. Jacobian matrix is used to approximate a small displacement in different spaces. Thus, the kinematic model from six DOF AUV is shown in Eq. (2) [27]:

$$\begin{bmatrix} v_1 \\ v_2 \end{bmatrix} = \begin{bmatrix} {J_1}^{-1}(\eta_2) & 0_{3\times3} \\ 0_{3\times3} & {J_2}^{-1}(\eta_2) \end{bmatrix} \begin{bmatrix} \dot{\eta}_1 \\ \dot{\eta}_2 \end{bmatrix} \Leftrightarrow v = J^{-1}(\eta)\dot{\eta} \quad (2)$$

where

$${J_1}^{-1}(\eta_2) = \begin{bmatrix} \cos\psi\cos\theta & -\sin\psi\cos\phi + \cos\psi\sin\theta\sin\phi & \sin\psi\sin\phi + \cos\psi\cos\phi\sin\theta \\ \sin\psi\cos\theta & \cos\psi\cos\phi + \sin\phi\sin\theta\sin\psi & -\cos\psi\sin\phi + \sin\theta\sin\psi\cos\phi \\ -\sin\theta & \cos\theta\sin\phi & \cos\theta\cos\phi \end{bmatrix}$$

$${J_2}^{-1}(\eta_2) = \begin{bmatrix} 1 & 0 & \sin\theta \\ 0 & \cos\phi & \cos\theta\sin\phi \\ 0 & -\sin\phi & \cos\theta\cos\phi \end{bmatrix}$$

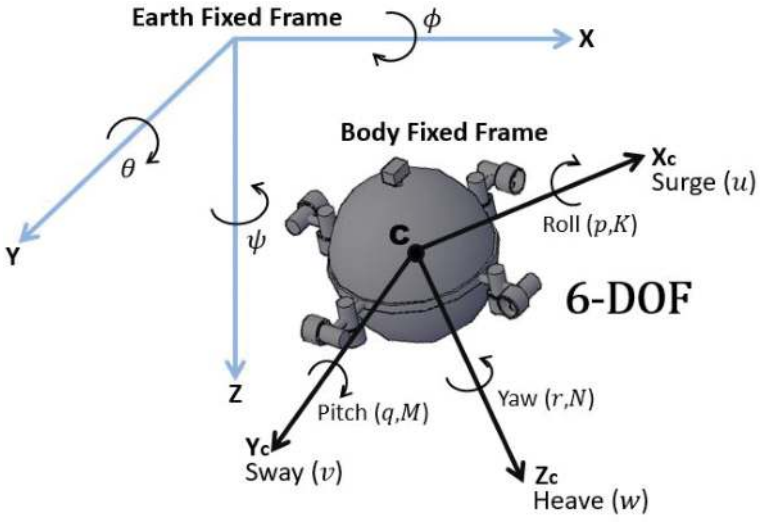

Figure 1. Body-fixed frame and earth fixed reference frame.

Meanwhile, the acceleration during a motion is studied by the dynamics model. The dynamic model is developed from the Newtonian and Lagrangian principles. This has been deeply discussed in Ref. [27]. The general dynamic model of the 6 DOFs AUV can be seen in Eq. (3):

$$M_{RB}\dot{v} + C_{RB}(v)v = \tau_{RB} \tag{3}$$

where $M_{RB} \in \mathbb{R}^{6\times6}$ is the inertia matrix of a rigid body AUV, $C_{RB} \in \mathbb{R}^{6\times6}$ is the coriolis and centripetal matrix of a rigid body, and $\tau_{RB} \in \mathbb{R}^{6\times1}$ is an external force and moment. However, the ocean is a rough area. The hydrodynamics effects inside the ocean move and rotate the AUV from the initial position. The hydrodynamics effect is a force caused by fluids. These effects should be considered to avoid a model error of the AUV. The examples of hydrodynamics effects are radiation-induced forces and environmental forces. The equation of the forces of the hydrodynamics effect is established in Eq. (4) [27]:

$$-M_A\dot{v} - C_A(v)v - D(v)v - g(\eta) = \tau_H \tag{4}$$

where M_A is the added inertial matrix, C_A is the added hydrodynamics coriolis and centripetal matrix, D is the potential damping matrix, g is the gravitational matrix influenced by restoring forces, and τ_H donates the hydrodynamics' forces.

Eliminate the external forces by the hydrodynamics effect as shown in Eqs. (5–7):

$$\tau_{RB} - \tau_H = \tau \tag{5}$$

$$(M_{RB} + M_A)\dot{v} + (C_{RB} + C_A)(v)v + D(v)v + g(\eta) = \tau \tag{6}$$

$$M\dot{v} + C(v)v + D(v)v + g(\eta) = \tau \tag{7}$$

where $M \in \mathbb{R}^{6\times6}$ indicates inertia matrix and added mass $(M_{RB} + M_A)$, $C(v) \in \mathbb{R}^{6\times6}$ is the coriolis and centripetal matrix and added mass $\Big(C_{RB}(v) + C_A(v)\Big)$, $D(v) \in \mathbb{R}^{6\times6}$ is the damping matrix (hydrodynamic damping and lift force), $g(\eta) \in \mathbb{R}^{6\times1}$ represents the gravitational force and moment (restoring force), and $\tau \in \mathbb{R}^{6\times1}$ is the control input/sum of estimated dynamics disturbances. Equation (2) is used to transform the dynamic model of AUV in Eq. (7) as follows,

$$M(\eta)\ddot{\eta} + C(v,\eta)\dot{\eta} + D(v,\eta)\dot{\eta} + g(\eta_2) = J^{-T}\tau \tag{8}$$

The dynamic model in Eq. (8) maintains Property 1, Property 2, and Property 3 [28].

Property 1 : M is symmetric and positive definite such that $M = M^T > 0$.

Property 2 : $C(v,\eta)$ is the skew-symmetric matrix such that $C(v,\eta) = -C^T(v,\eta)$.

Property 3 : $D(v,\eta)$ is positive definite, that is, $D(v,\eta) = D^T(v,\eta) > 0$.

3. Proposed control

This section discusses a proposed control which combines the super twisting sliding mode and region boundary scheme for a six-DOF AUV. Some equations in region boundary are used in super twisting sliding mode control; hence, this method is explained earlier.

http://dx.doi.org/10.5772/67579

3.1. Super twisting sliding mode controller

Super twisting is a part of the high order sliding mode control (HOSMC). The basic idea of HOSMC is removing the chattering effect, increasing the accuracy for tracking trajectory, and at the same time maintaining the advantages of conventional SMC [16]. In the conventional SMC, the control law consists of discontinuous system to ensure a sliding regime and the error convergence in a finite time happens when the system is restricted in the sliding surface. However, the high switching frequency known as chattering effect in the output signal is produced, thus, the stability of the control system is disturbed [29]. Furthermore, the value of sliding surface cannot be zero if the switching error exists. For this reason, super twisting SMC is used to preserve the zero value of sliding surface although in the presence of switching error [30].

There are two components in the super twisting SMC, the derivative of the discontinuous sliding surface and the continuous function of the sliding variable. Formulating the continuous function is useful to handle the chattering effect produced by the discontinuous function. The super twisting SMC is shown in Eq. (9):

$$\tau_{st} = \tau_1 + \tau_2 \tag{9}$$

where τ_1 denotes the discontinuous time derivative and τ_2 is a continuous function of the sliding variable. The values of τ_1 and τ_2 are determined in Eqs. (10) and (11), respectively:

$$\tau_1 = \int -\mathrm{K}\, sgn\,(s) \tag{10}$$

$$\tau_2 = -\kappa |s|^{0.5}\, sgn\,(s) \tag{11}$$

where s is the sliding surface, $\mathrm{K} \in \mathbb{R}$ represents a control parameter of the discontinuous system and its value is greater than zero, $\kappa \in \mathbb{R}$ represents a gain of continuous system, and sgn is a signum symbol. The value of $sgn\,(s)$ is equal to -1 if the sliding surface is less than zero, equal to zero if the sliding surface is zero, and equal to 1 if the sliding surface is greater than zero. The sliding surface is defined based on the first derivative of the tracking error, as shown in Eq. (12),

$$s = \dot{\eta} - \dot{\eta}_r \tag{12}$$

where $\dot{\eta}$ denotes the actual velocity and η_r denotes the reference vector which is developed from the region-based control. The final equation of super twisting sliding mode controller is given in Eq. (13):

$$\tau_{st} = \int -\mathrm{K}\, sgn\,(s) - \kappa |s|^{0.5}\, sgn\,(s) = \int -\mathrm{K}\, sgn\,(\dot{\eta} - \dot{\eta}_r) - \kappa |\dot{\eta} - \dot{\eta}_r|^{0.5}\, sgn\,(\dot{\eta} - \dot{\eta}_r) \tag{13}$$

Remark 3.1: Equation (13) reaches the finite time convergence as long as $\mathrm{K} > \frac{d}{\Gamma_M}$ and $\kappa^2 \geq \frac{4d\Gamma_M(\mathrm{K}+d)}{\Gamma_m^2\Gamma_m(\mathrm{K}+d)}$, where d is an arbitrary chosen as a positive real number of disturbance, Γ_m and Γ_M are constants with $\Gamma_m = \mathrm{K} - d_0$ and $\Gamma_M = \mathrm{K} + d_0$, while d_0 denotes the initial value of d.

3.2. Region boundary scheme

The region boundary scheme works by replacing line-based into region-based trajectory and different shapes of region can be decided by choosing the appropriate function [24]. The objective region in an inequality functions is given as follows,

$$f_i(\Delta\eta_i) = \begin{bmatrix} f_1(\Delta\eta_1) \\ f_2(\Delta\eta_2) \\ \cdots \\ f_N(\Delta\eta_N) \end{bmatrix} \leq 0 \tag{14}$$

where $\Delta\eta_i \triangleq (\eta - \eta_d) \in \mathbb{R}^3$, i is declared as 1, 2, …, N with N being the total number of objective function, $\eta \in \mathbb{R}^3$ is an actual position/orientation of an AUV, and $\eta_d \in \mathbb{R}^3$ is a reference point of $f_i(\Delta\eta_i)$. The actual position of an AUV is counted from the position of origin C of the vehicle. The example of region boundary scheme is explained as follows: the desired region is determined as a 2D square, the illustration is shown in **Figure 2**. The inequality function of **Figure 2** is given as

$$\begin{aligned} f_1(\Delta\eta_1) &= (x - x_d)^2 - r_x^2 \leq 0 \\ f_2(\Delta\eta_2) &= (y - y_d)^2 - r_y^2 \leq 0 \end{aligned} \tag{15}$$

where r_x and r_y are the regional bound.

To calculate the energy consumption when the AUV tracks on the region, the inequality function in Eq. (14) should be modified by adding the potential energy, given in Eq. (16):

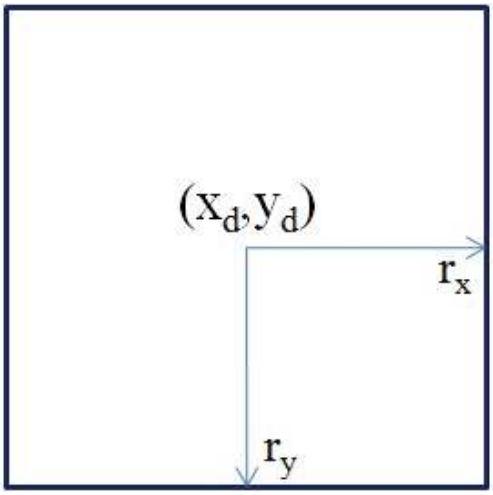

Figure 2. Rectangle desired region.

http://dx.doi.org/10.5772/67579

$$P(\Delta\eta) = \sum_{i=1}^{N} P_i(\Delta\eta_i) \tag{16}$$

where $P_i(\Delta\eta) \triangleq \frac{k_{pi}}{2}\left[\max(0, f_i(\Delta\eta))\right]^2$. The value of $P_i(\Delta\eta_i)$ relies on Eq. (17):

$$P_i(\Delta\eta_i) = \begin{cases} 0 & , \text{ if } f_i(\Delta\eta_i) \le 0 \\ \frac{k_{pi}}{2} f_i^2(\Delta\eta) & , \text{ if } f_i(\Delta\eta_i) > 0 \end{cases} \tag{17}$$

where $k_p \in \mathbb{R}^{N\times N}$ denote positive constants of the potential energy. Note that the value of $f_i(\Delta\eta_i)$ is less than or equal to zero when the AUV enters the bound, thus, the gradient of $P_i(\Delta\eta_i)$ becomes smaller. Then, differentiating Eq. (17) with respect to $\Delta\eta_i$ yields Eq. (18):

$$\left(\frac{\partial P(\Delta\eta)}{\partial \Delta\eta}\right)^T = \sum_{i=1}^{N} k_{Pi} \max\left(0, f_i(\Delta\eta_i)\right)\left(\frac{\partial f_i(\Delta\eta_i)}{\partial \Delta\eta_i}\right)^T \triangleq \Delta e_\eta \tag{18}$$

where Δe_η is the region error whose value reduces to zero once the AUV move toward the desired region [24].

Remark 3.2: The region error will trigger an AUV toward the desired region. Once the AUV is inside the region, the gradient of potential energy, $P_i(\Delta\eta_i)$, becomes zero and at the same time Δe_η reduces smoothly to zero.

3.3. Super twisting sliding mode controller with region boundary scheme

Equation of super twisting SMC with region boundary scheme is shown in Eq. (19):

$$\tau = \tau_{st} + \tau_{eq} \tag{19}$$

where τ denotes a force acting on the center mass of an AUV or a control input, τ_{st} is a super twisting SMC, and τ_{eq} is the energy saving control law. Differentiating a sliding surface in Eq. (12) with respect to time yields Eq. (20):

$$\dot{s} = \ddot{\eta} - \ddot{\eta}_r \tag{20}$$

The following equation is the reference vector according to the region error,

$$\dot{\eta}_r = J^{-1}(\eta)(\dot{\eta}_d - \Delta\eta) - \alpha J^{-1}(\eta)\Delta e_\eta \tag{21}$$

where α is a constant value and $\Delta\eta$ represents the difference value between the actual and the desired position. Second derivatives of Eq. (21) with respect to time produces Eq. (22) [24]:

$$\ddot{\eta}_r = \dot{J}^{-1}(\eta)(\dot{\eta}_d - \Delta\eta) + J^{-1}(\eta)(\ddot{\eta}_d - \Delta\dot{\eta}) - \alpha\dot{J}^{-1}(\eta)\Delta e_\eta - \alpha J^{-1}(\Delta\dot{e}_\eta) \tag{22}$$

Then, multiplying M into both sides of Eq. (20) yields

$$M\dot{s} = M\ddot{\eta} - M\ddot{\eta}_r \tag{23}$$

where $M\ddot{\eta} = J^{-T}\tau_{eq} - (C\dot{\eta} + D\dot{\eta} + g)$. Determine $\dot{s} = 0$, hence [24]

$$M\dot{s} = J^{-T}\tau_{eq} - (M\ddot{\eta}_r + C\dot{\eta} + D\dot{\eta} + g)\tau_{eq} = J^T(M\ddot{\eta}_r + C\dot{\eta} + D\dot{\eta} + g) \tag{24}$$

Substitute $J^T\Delta e_\eta$ into Eq. (24), thus, energy saving potential control is obtained in Eq. (25) [24]:

$$\tau_{eq} = J^T(M\ddot{\eta}_r + C\dot{\eta} + D\dot{\eta} + g) - J^T\Delta e_\eta \tag{25}$$

Remark 3.3: Energy saving potential control drives the sliding surface converging to zero throughout the tracking mission, thus the AUV tracks inside the region.

Finally, super twisting SMC based on region boundary scheme is shown in Eq. (26):

$$\tau = \int \Big(- \mathrm{K}\, sgn\,(\dot{\eta} - \dot{\eta}_r)\Big) - \kappa|(\dot{\eta} - \dot{\eta}_r)|^{0.5}\, sgn\,(\dot{\eta} - \dot{\eta}_r) + J^T(M\ddot{\eta}_r + C\dot{\eta} + D\dot{\eta} + g) - J^T\Delta e_\eta \tag{26}$$

Theorem: The control input τ in Eq. (26) minimizes the chattering effect and allows the AUV to track on the desired region under determined perturbations as long as Remarks 3.1, 3.2, and 3.3 are fulfilled. Hence, the global asymptotic stability of closed loop systems is also guaranteed.

Proof: Propose a positive definite function of a Lyapunov candidate given in Eq. (27):

$$V = \frac{1}{2}s^TMs + \sum_{i=1}^{N} k_{Pi}\max\Big(0, f_i(\Delta\eta_i)\Big)\left(\frac{\partial f_i(\Delta\eta_i)}{\partial\Delta\eta_i}\right)^T + 2\kappa|s| + \frac{1}{2}{\tau_1}^2 + \frac{1}{2}\Big(\mathrm{K}|s|^{\frac{1}{2}}\, sgn\,(s) - \tau_1\Big)^2 \tag{27}$$

Define ζ equal to $\begin{bmatrix} |s|^{\frac{1}{2}}\, sgn\,(s) & \tau_1 \end{bmatrix}^T$ and $\overline{P}$ equal to $\frac{1}{2}\begin{bmatrix} 4\kappa + \mathrm{K}^2 & -\mathrm{K} \\ -\mathrm{K} & 2 \end{bmatrix}$. Equation (27) is transformed as a quadratic form as shown in Eq. (28):

$$V = \frac{1}{2}s^TMs + \sum_{i=1}^{N} k_{Pi}\max\Big(0, f_i(\Delta\eta_i)\Big)(\Delta\dot{\eta})^T\left(\frac{\partial f_i(\Delta\eta_i)}{\partial\Delta\eta_i}\right)^T + \zeta^T\overline{P}\zeta \tag{28}$$

Differentiating Eq. (28) with respect to time yields

$$\dot{V} = s^TM\dot{s} + \sum_{i=1}^{N} k_{Pi}\max\Big(0, f_i(\Delta\eta_i)\Big)(\Delta\dot{\eta})^T\left(\frac{\partial f_i(\Delta\eta_i)}{\partial\Delta\eta_i}\right)^T - \frac{1}{|s^{1/2}|}\zeta^TQ\zeta + {q_1}^T\zeta \tag{29}$$

where $Q = \frac{\mathrm{K}}{2}\begin{bmatrix} 2\kappa + \mathrm{K}^2 & -\mathrm{K} \\ -\mathrm{K} & 1 \end{bmatrix}$ and ${q_1}^T = \begin{bmatrix} 2\kappa + \frac{1}{2}\mathrm{K}^2 & -\frac{1}{2}\mathrm{K} \end{bmatrix}$. Substituting Eq. (24) into Eq. (29) gives [18]

http://dx.doi.org/10.5772/67579

$$\dot{V} = s^T\left(J^{-T}\tau - (M\ddot{\eta}_r + C\dot{\eta} + D\dot{\eta} + g)\right) + \sum_{i=1}^{N} k_{Pi}\max\left(0, f_i(\Delta\eta_i)\right)(\Delta\dot{\eta})^T\left(\frac{\partial f_i(\Delta\eta_i)}{\partial\Delta\eta_i}\right)^T - \frac{W}{2|s^{1/2}|}\zeta^T\tilde{Q}\zeta \tag{30}$$

where δ denotes coefficient of perturbation and $\tilde{Q} = \begin{bmatrix} 2\kappa + \mathrm{K}^2 - \left(\frac{4\kappa}{\mathrm{K}} + \mathrm{K}\right)\delta & -\mathrm{K} + 2\delta \\ -\mathrm{K} + 2\delta & 1 \end{bmatrix}$.

Assume τ_{eq} in Eq. (25) as τ and substitute into Eq. (30), hence,

$$\dot{V} = -s^T(\Delta e_\eta) + \sum_{i=1}^{N} k_{Pi}\max\left(0, f_i(\Delta\eta_i)\right)(\Delta\dot{\eta})^T\left(\frac{\partial f_i(\Delta\eta_i)}{\partial\Delta\eta_i}\right)^T - \frac{\mathrm{K}}{2|s^{1/2}|}\zeta^T\tilde{Q}\zeta \tag{31}$$

$$\dot{V} = -\left(\dot{\eta} - J^{-1}(\eta)(\dot{\eta} - \Delta\eta) - \alpha J^{-1}(\eta)\Delta e_\eta\right)(\Delta e_\eta) + \sum_{i=1}^{N} k_{Pi}\max\left(0, f_i(\Delta\eta_i)\right)(\Delta\dot{\eta})^T\left(\frac{\partial f_i(\Delta\eta_i)}{\partial\Delta\eta_i}\right)^T - \frac{\mathrm{K}}{2|s^{1/2}|}\zeta^T\tilde{Q}\zeta \tag{32}$$

$$\dot{V} \leq -\alpha\Delta e_\eta{}^T\Delta e_\eta - \frac{\mathrm{K}}{2|s^{1/2}|}\zeta^T\tilde{Q}\zeta \leq 0 \tag{33}$$

V is bounded since M is uniformly positively definite, hence, s and $P_i(\Delta\eta_i)$ are also bounded. By applying Barbalat's Lemma and Remark 3.1, it implies that $\dot{V}$ is negative definite if $\tilde{Q} > 0$. Therefore, the proposed control for the dynamic system of AUV in Eq. (7) guarantees $\Delta e_\eta \to 0$ and $s \to 0$ in $t \to \infty$. Region error converges to zero indicates that $f_i(\Delta\eta_i) \leq 0$, thus, $\frac{\partial f_i(\Delta\eta_i)}{\partial\Delta\eta_i}$ converges to zero.

3.4. Related control laws for comparative analysis

Because of the similarity of the proposed controller, some controller such as conventional sliding mode control (SMC), fuzzy SMC, and super twisting SMC are selected for the comparison purpose in the simulation. The equation of each comparison control is discussed as follows.

3.4.1. Sliding mode control (SMC)

The function of SMC is shown in Eq. (34) [5],

$$\tau_{\mathrm{SMC}} = -\mathrm{K}\, sgn\,(s) + \int k_s\, \dot{\eta}_r \tag{34}$$

The sliding surface s, $\dot{\eta}_r$, and $\Delta\eta$ are defined as follows

$$s = \dot{\eta} - \dot{\eta}_r \tag{35}$$

$$\dot{\eta}_r = J^{-1}(\eta)(\dot{\eta}_d - \Delta\eta) \tag{36}$$

$$\Delta\eta = \eta - \eta_d \tag{37}$$

where $k_s \in \mathbb{R}$ is a constant of integrate controller.

3.4.2. Fuzzy SMC

Formula of fuzzy SMC is given in Eq. (38) [31]

$$\tau_{\text{fuzzy}} = -\mathrm{K}_f \; sgn\,(s) + \int k_s \; \dot{\eta}_r \tag{38}$$

where $\mathrm{K}_f \in \mathbb{R}$ indicates the control parameter of discontinuous system which is obtained from the fuzzy rule, $k_s \in \mathbb{R}$ is a constant of an integrate controller, while the value of s, $\dot{\eta}_r$, and $\Delta\eta$ are the same as Eqs. (35), (36), and (37). The rule of fuzzy is given in **Table 1**, where s and $\dot{s}$ are the input of membership function and K_f is the output. Input s uses a trim type of membership function and its value varies from −150 to 150, input $\dot{s}$ uses the same type as s and its value varies from -1×10^{10} to 1.5×10^{10}, while output K_f uses *gauss2mf* as the type of membership function with range value from 5 to 25. The graph of the membership function is shown in **Figure 3**.

3.4.3. Super twisting SMC

The formula of super twisting SMC is given in Eq. (39) [32]

$$\tau_{\text{ST}} = \int -\mathrm{K}\; sgn\,(s) - \kappa|s|^{0.5}\; sgn\,(s) \tag{39}$$

where $\mathrm{K} \in \mathbb{R}$ is a control parameter of discontinuous system and $\kappa \in \mathbb{R}$ is a constant of continuous system. Equations (35–37) are used as the value of s, $\dot{\eta}_r$, and $\Delta\eta$.

		s						
K_f		**Negative large**	**Negative medium**	**Negative small**	**Zero**	**Positive small**	**Positive medium**	**Positive large**
$\dot{s}$	Negative	Large	Large	Large	Medium	Small	Medium	Large
	Zero	Large	Large	Medium	Small	Medium	Large	Large
	Positive	Large	Medium	Small	Medium	Large	Large	Large

Table 1. Fuzzy rule.

http://dx.doi.org/10.5772/67579

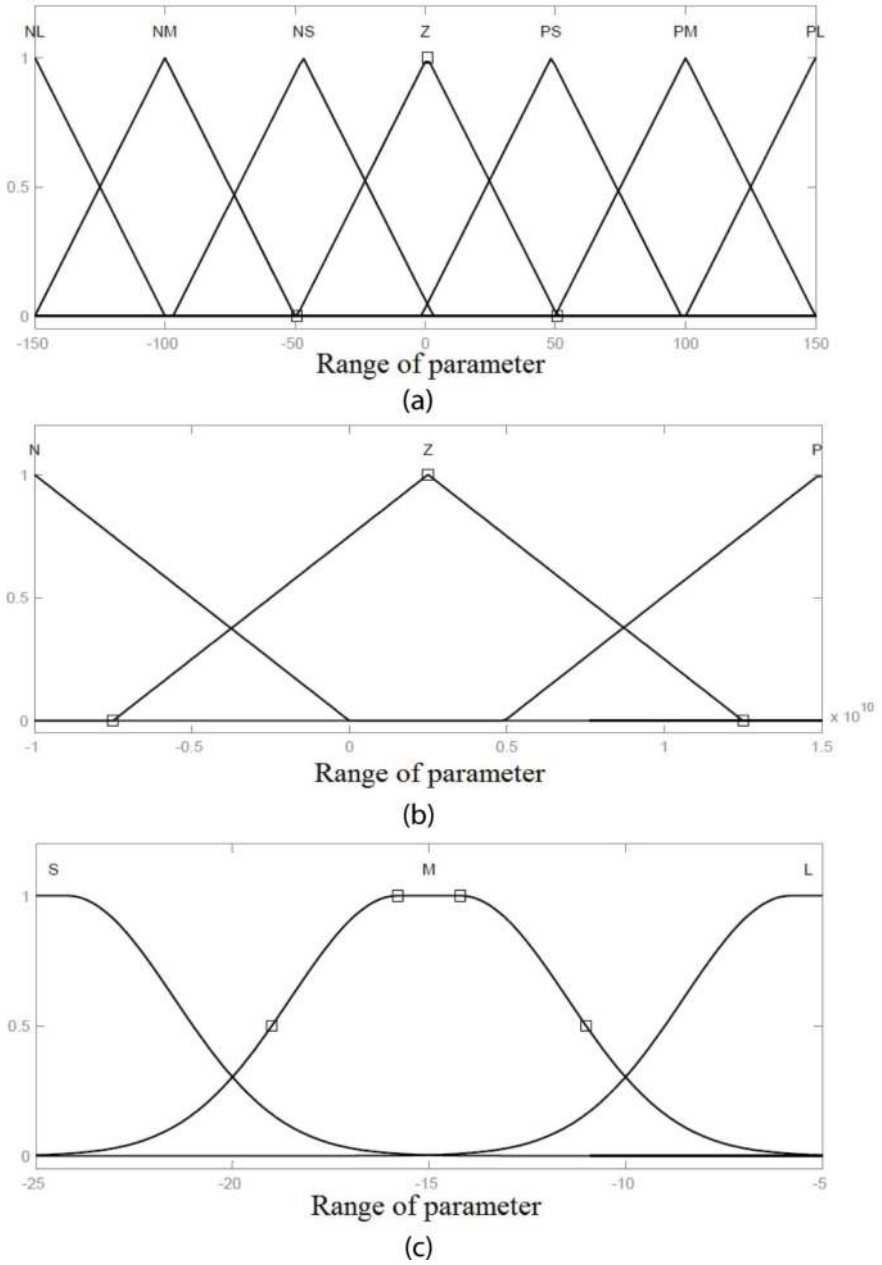

Figure 3. Membership function plot of fuzzy for (a) input s, (b) input $\dot{s}$ and (c) output K_f.

4. Results

The simulation utilizes an omni-directional intelligent navigator (ODIN) type of an AUV developed by Hawaii University as it is easy and widely used for the simulation purpose, as well as a holonomic model so that the singularity can be avoided and capable to move in six degree of freedoms (DOFs) without any preference of direction [33, 34]. The ODIN has eight thrusters to support its movement and does not require a heading angle to achieve a certain position. The horizontal diameter of an ODIN is 0.63 (m), while the vertical diameter is 0.61 (m). Its dry weight is about 125 (kg). There are two types of trajectories, which will be used in the simulation, a conventional line trajectory and a region trajectory. The conventional trajectory is applied on the conventional sliding mode control (SMC), fuzzy SMC, and super twisting SMC, while the region trajectory determined as a spherical shape is applied on the proposed control. An AUV is placed in the initial position at $[0 \quad 1 \quad 0]^{\mathrm{T}}$m, then it moves to the start sign at $[1.5 \quad 0 \quad -1.2]^{\mathrm{T}}$m, which indicates the start-tracking point, while the finish sign is at $[10 \quad 0 \quad 0]^{\mathrm{T}}$m where the simulation is stopped. The inequality equation of the spherical region is shown in Eq. (40) [25]:

$$f(\Delta\eta_1) = (x - x_d)^2 + (y - y_d)^2 + (z - z_d)^2 - r^2 \leq 0 \tag{40}$$

where $(x,\ y,\ z)$ represents the position of the vehicle in the x, y, and z axes, $(x_d,\ y_d,\ z_d)$ denotes the centre of the spherical region, and $r = 0.2$ m is the radius of the desired region. The value of the radius is determined arbitrary bigger than the radius of the ODIN, and there is no specific term on how to determine the value of the radius [24]. In the middle of the tracking activity, $0.05\ \mathrm{ms}^{-1}$ linear perturbation on x-axis, y-axis, and z-axis disturb the movement of an AUV. **Table 2** shows the parameter's values for each controller.

The first result is shown about tracking performance to see whether the AUV tracks outside the trajectory. As shown in the result of the conventional SMC in **Figure 4(a)**, the AUV reached the desired position after it moved down and gave oscillations of around 30 s at the start of the tracking point. Slightly similar to the conventional SMC, the AUV under the fuzzy SMC, shown in **Figure 4(b)**, also moved down before it reached the desired position, although the

No.	Controller	Parameter	
1.	Proposed controller	$\kappa = 14.5$	$\mathrm{K} = 0.5$ $\alpha = 0.3$ $k_{pi} = \mathrm{diag}\{1,\ 1,\ 1\}$
2.	Conventional SMC	$\mathrm{K} = 20$ $k_s = 0.01$	
3.	Fuzzy SMC	Input = s and $\dot{s}$ Output K_f from 5 to 25 $k_s = 0.01$	
4.	Super twisting SMC	$\kappa = 25$	$\mathrm{K} = 5$ $k_s = 0.01$

Table 2. Technical description.

http://dx.doi.org/10.5772/67579

oscillations did not appear. A better performance was shown under the super twisting SMC which can be seen in **Figure 4(c)**. The AUV moved slightly straight toward the start tracking point from the initial position. The oscillations also did not appear under this controller. However, the proposed controller gave the best movement compared to the others. From **Figure 4(d)**, the AUV moved straight from the initial position to the start tracking point. In the perturbation time, it is shown that the higher the value of the perturbation, the further the AUV moved from its desired position. While **Figure 4(a)–(c)** show that the AUV was unable to maintain its position on the tracking line, the opposite result is shown in **Figure 4(d)**. The AUV remains inside the region boundary even though the perturbations are presented.

Next, results are discussed about error convergence and analyzed how long the controller takes the AUV to settle from the perturbation's effect. The time is counted from $\eta \neq 0$ to $\eta = 0$. $\eta \neq 0$ indicates the AUV is not on the desired position. In the case of the proposed controller, the error convergence is counted from $\eta \neq r$ to $\eta < r$. "r" sign indicates the radius of region boundary or the allowable error of the AUV's position based on Eq. (40), while $\eta < r$ indicates that the AUV has been inside the region. Another aim of error convergence is to see whether the controller produces the chattering effect during the convergence. **Figures 5(a)** and **(b)**

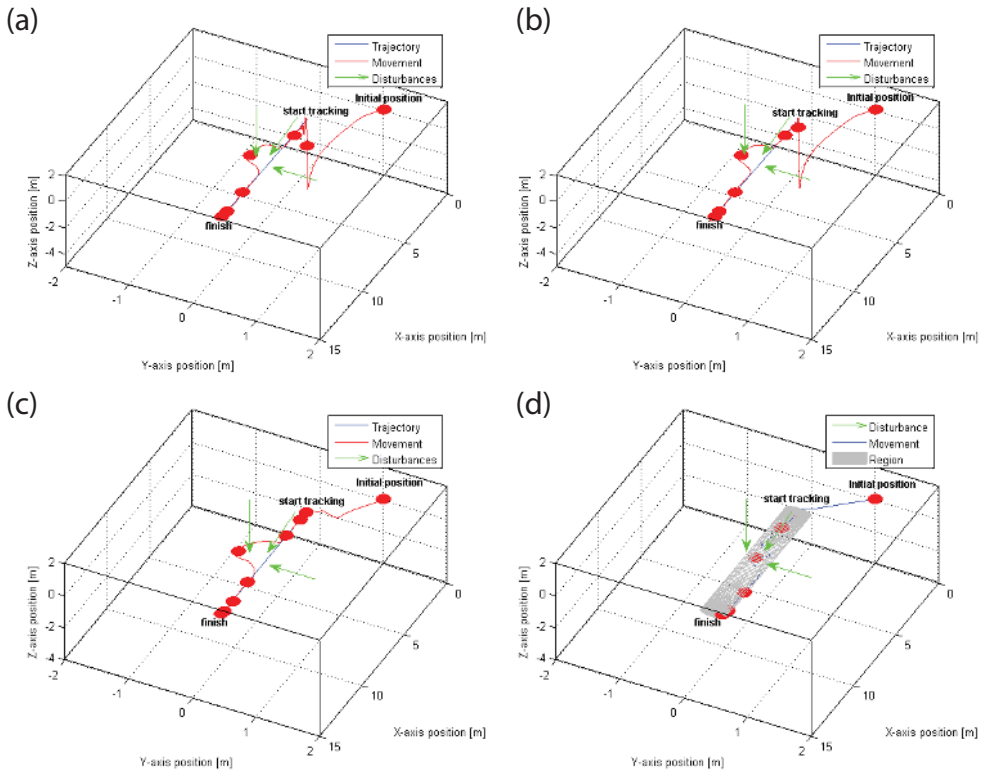

Figure 4. 3D results for (a) conventional SMC, (b) fuzzy SMC, (c) super Twisting SMC, and (d) proposed controller.

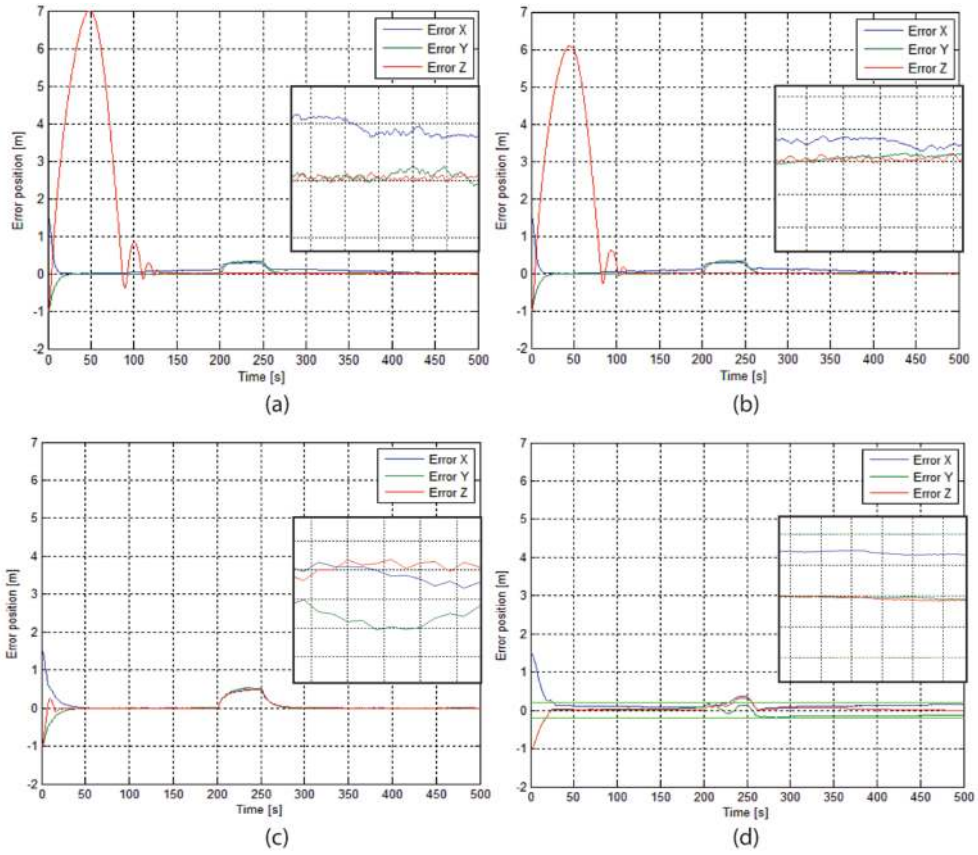

Figure 5. Error convergence for (a) conventional SMC, (b) fuzzy SMC, (c) super twisting SMC, and (d) proposed controller.

show that the *X*- and *Y*-axes of conventional SMC and fuzzy SMC converged to zero faster than the *Z*-axis in the beginning of the time. The *X*- and *Y*-axes of conventional SMC took 5 s and 125 s was needed by *Z*-axis. Meanwhile, the *X*- and *Y*-axes of fuzzy SMC required 27 s to make the AUV converge to the desired trajectory and 118 s were needed by the *Z*-axis. Conventional SMC and fuzzy SMC took a longer time to converge to zero due to the increasing value of perturbations. The time required for the error convergence in the *X*- and *Y*-axes was 180 s, while 15 s was required for the *Z*-axis. Meanwhile, the super twisting SMC required 30 s for the error convergence in all axes, while 5 s was required by the proposed controller during the perturbation time. The maximum error for the conventional SMC, fuzzy SMC, super twisting SMC, and the proposed controllers was 0.3, 0.3, 0.4, and 0.02 m, respectively. Meanwhile, the small graph of **Figures 5(a)** and **(b)** show the conventional SMC and fuzzy SMC producing the chattering in the presence of perturbation. A small chatter is also shown by super twisting SMC in small graph of **Figure 5(c)**, while proposed control showed a stable signal as performed in small graph of **Figure 5(d)**.

http://dx.doi.org/10.5772/67579

Results of force and moment are accumulated to obtain the energy spent by the AUV when the mission is executed. Force is an energy to make an object, in this case an AUV, move linearly from its initial position. On the other hand, moment is a force to make an AUV rotate from its center. The value of the force and moment were collected within the perturbed time or when the perturbations started to disturb the AUV. The reason for selecting this specific time was to see the differences in the way each controller handled the same perturbation. High amounts of force and moment indicate the inefficiency of the controller. The total amount was calculated by using the two-norm function or Euclidean distance and was considered as the energy spent by the AUV to accomplish the desired mission. As shown in **Table 3**, the proposed control spent the least energy at 356.72 N for force and at 65.02 Nm for moment compared to other controllers. The highest amount of force is spent by super twisting SMC at 463.45 N, while conventional SMC spent the highest amount of moment at 449.58 Nm.

The last results discuss about the thrusters' distribution. These data are collected to analyze the effort of the propeller to maintain the AUV at its desired position. The more effort spent by the propeller, the more power will be consumed. The ODIN had eight thrusters to move the AUV from one place to another. The eight thrusters were divided into two functions. Thrusters 1–4 were used to move the AUV horizontally, while thrusters 5–8 were used to move it vertically. **Figure 6** shows that the oscillation values of all the thrusters for conventional SMC and fuzzy SMC were similar. For super twisting SMC, more effort was required by thrusters 1, 3, 7, and 8 in the presence of disturbances, while the other thrusters showed constant oscillation. In the case of a proposed controller, all thrusters required more effort when the AUV was disturbed by perturbation.

It can be seen from the results that the proposed controller gave the best performance in terms of robustness and energy consumption. The first was referred from the value of the gain selection. The proposed controller needed smaller parameters value, 14.5 of κ and 0.5 of κ, compared to the other controllers. These parameters were used to trigger the movement of the AUV toward the desired position or were related to the tracking performance and error convergence. In normal situations, a high value of this parameter results in oscillations at the beginning of the time. In contrast, a small value of this parameter causes the AUV to take a longer time to reach the target. The worst case is the AUV never reaches the target. Second discussion is about error convergence. The results of the error convergence showed that all the controllers, except for the proposed controller, produced oscillations at the beginning of the time. The highest oscillation was produced by the conventional SMC, followed by the fuzzy SMC and the super twisting SMC. Hence, the AUV could not move directly from the initial position to the start tracking point under the conventional SMC and fuzzy SMC. Zero error convergences exist in the case of line trajectory for conventional SMC, fuzzy SMC, and super twisting SMC. Different result was shown in the use of region trajectory as the error position

Control	SMC	Fuzzy SMC	Super twisting SMC	Proposed control
Force	442.45 N	440.13 N	463.45 N	356.72 N
Moments	449.58 Nm	463.97 Nm	172.27 Nm	65.02 Nm

Table 3. Norm value of force and moment.

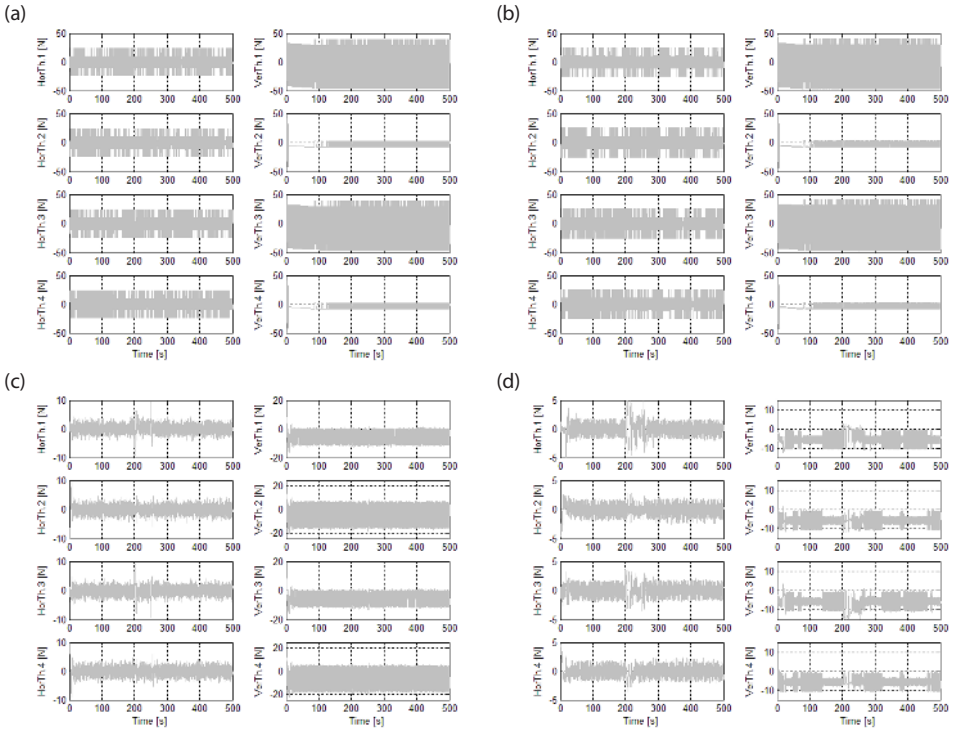

Figure 6. Thrusters' distribution for (a) conventional SMC, (b) fuzzy SMC, (c) super twisting SMC, and (d) proposed controller.

converged to the determined radius or allowable error instead of zero. This condition is in accordance with Remark 3.2 that as long as the AUV is inside the region, the gradient of potential energy becomes zero, thus the error region reduces to zero. According to the proof, one condition to ensure $s \rightarrow 0$ is the error convergence into region boundary.

In terms of the time required for the error convergence, the proposed controller took the shortest time to converge to zero, followed by the super twisting SMC. The position of the AUV at each axis under the conventional SMC and fuzzy SMC could not converge simultaneously. In this case, the time requirement stops had to be calculated when the position of the AUV in all the axes converged to zero. Thus, the conventional SMC took the longest time to converge to zero, followed by the fuzzy SMC. It could be seen from the results of the tracking performance that the AUV managed to move within the region under the proposed controller in the presence of perturbation. On the other hand, the other controllers failed to maintain the position of the AUV on the desired tracking line.

Based on the energy consumption, the super twisting SMC spent the highest force, both under constant and sine wave Gaussian white noise perturbations. The conventional SMC and fuzzy SMC were in the middle position, while the proposed controller spent the least force. The

http://dx.doi.org/10.5772/67579

proposed control saved up to 30.2% of linear force consumption. For the moment under the constant perturbations, the highest value was spent by the conventional SMC, followed by the fuzzy SMC, the super twisting SMC, and the proposed controller. Meanwhile, the highest moment value under the sine wave Gaussian white noise perturbation was spent by the fuzzy SMC, followed by the conventional SMC, the super twisting SMC, and the proposed controller. In this case, the proposed controller saved more than 50% of the moment consumption.

More force was spent by the super twisting SMC and the proposed controller during the transition from the initial point. Therefore, the AUV was enabled to move directly to the start tracking point. These controllers also reacted to the presence of perturbations. The higher the value of the perturbation that disturbed the AUV, the greater the force that would be spent. In contrast, the conventional SMC and the fuzzy SMC showed a similar pattern of force and moment in all the times and in all conditions. This meant that these two controllers were not able to adapt well in handling changes in the situation.

The last discussion is about the propulsion or distribution of the thrusters. The proposed controller produced the least effort during the mission, followed by the super twisting SMC. Meanwhile, the conventional SMC and the fuzzy SMC showed the most active propulsion in all conditions. This situation was not good due to the battery consumption of the AUV. The more active thrusters indicated that the AUV would lose battery power easily. The high value of propulsion of the thrusters was also not good for the electrical devices inside the AUV.

5. Conclusion

A new robust-region-based controller is introduced from a survey of existing robust controls and saving energy approach for an autonomous underwater vehicle (AUV). Lyapunov candidate was used to prove a global asymptotical stability, while some simulations involving conventional sliding mode control (SMC), fuzzy SMC, and the only use of super twisting SMC were conducted under two kinds of perturbations to observe the effectiveness of the proposed controller. It is shown that the use of proposed controller was able to keep the AUV within the desired region under certain value of constant perturbations as well as a sinusoidal perturbation with a Gaussian white noise. From the results, it can be concluded that the proposed controller was able to minimize the chattering effect, provide a good response when overcoming the disturbances, provide a short computational time of error convergence, and save the amount of force and moment.

Author details

Vina Wahyuni Eka Putranti and Zool Hilmi Ismail*

*Address all correspondence to: zool@utm.my

Centre for Artificial Intelligence & Robotics, Universiti Teknologi Malaysia, Kuala Lumpur, Malaysia

References

[1] Joshi, S. D. and Talange, D. B. Performance Analysis: PID and LQR Controller for REMUS Autonomous Underwater Vehicle (AUV) Model. International Journal of Electrical Engineering & Technology (IJEET). 2012. 3(2): 320–327.

[2] Wadoo, S. A., Sapkota, S. and Chagachagere, K. Optimal Control of an Autonomous Underwater Vehicle. Systems, Applications and Technology Conference (LISAT), 2012. IEEE Long Island, Farmingdale, NY, 1–6.

[3] Nguyen, Q. H. and Kreuzer, E. A Robust Adaptive Sliding Mode Controller for Remotely Operated Vehicles. Technische Mechanik. 2007. 28(3–4): 185–193.

[4] Cristi, R., Papoulias, F. A. and Healey, A. J. Adaptive Sliding Mode Control of Autonomous Underwater Vehicles in The Dive Plane. IEEE Journal of Oceanic Engineering. 2002. 15(3): 152–160.

[5] Hong, E. Y., Soon, H. G. and Chitre, M. Depth Control of an Autonomous Underwater Vehicle, STARFISH. OCEANS 2010 IEEE. Sydney, 1–6.

[6] Akçakaya, H., Yildiz, H. A., Salam, G. and Gürleyen, F. Sliding Mode Control of Autonomous Underwater Vehicle. International Conference on Electrical and Electronics Engineering, 2009. ELECO 2009. November 5–8, 2009. Bursa: IEEE. 2009. II-332-II-336.

[7] Yildiz, O., Gokalp, R. B. and Yilmaz, A. E. A Review on Motion Control of the Underwater Vehicles. In: Proceedings of Electrical and Electronics Engineering, 2009. Bursa, 337–341.

[8] Guo, J., Chiu, F. C. and Huang, C. C. Design of a Sliding Mode Fuzzy Controller for The Guidance and Control of an Autonomous Underwater Vehicle. Ocean Engineering. 2003. 30(16): 2137–2155.

[9] Lakhekar, G. V. and Saundarmal, V. D. Novel Adaptive Fuzzy Sliding Mode Controller for Depth Control of an Underwater Vehicles. IEEE International Conference on Fuzzy Systems (FUZZ), 2013. July 7–10, 2013. Hyderabad: IEEE. 2013, 1–7.

[10] Van de Ven, P. W. J., Johansen, T. A., Sørensen, A. J., Flanagan, C. and Toal, D. Neural Network Augmented Identification of Underwater Vehicle Models. Control Engineering Practice. June 2007. 15(6): 715–725.

[11] Van de Ven, P. W. J., Flanagan, C. and Toal, D. Neural Network Control of Underwater Vehicles. Engineering Applications of Artificial Intelligence. August 2005. 18(5): 533–547.

[12] Li, J. H., Lee, P. M., Hong, S. W. and Lee, S. J. Stable Nonlinear Adaptive Controller for an Autonomous Underwater Vehicle Using Neural Networks. International Journal of Systems Science. 2007. 38(4): 327–337.

[13] Miao, B., Li, T. and Luo, W. A Novel Approach to Robust Adaptive NN Tracking Control for AUVs. 2014 33rd Chinese Control Conference (CCC), Nanjing. July 28–30, 2014. 8011–8016.

http://dx.doi.org/10.5772/67579

[14] Yuh, J. Learning Control for Underwater Robotic Vehicles. IEEE Control System Magazine. 1994. 14(2): 39–46.

[15] Levant, A. Higher-Order Sliding Modes, Differentiation and Output-Feedback Control. International Journal Control. 2003. 76(9–10): 924–941.

[16] Levant, A. Homogeinity Approach to High-Order Sliding Mode Design. Automatica. 2005. 41: 823–830.

[17] Moreno, J. A. and Osorio, M. A Lyapunov Approach to Second-Order Sliding Mode Controllers and Observers. 47th IEEE Conference on Decision and Control, 2008. CDC 2008. December 9–11, 2008. Cancun: IEEE. 2008. 2856–2861.

[18] Shtessel, Y. B., Moreno, J. A., Plestan, F., Fridman, L. M. and Poznyak, A. S. Super-Twisting Adaptive Sliding Mode Control: A Lyapunov Design. 49th IEEE Conference on Decision and Control, 2008. CDC 2008. December 15–17, 2010. Atlanta, GA: IEEE. 2010. 5109–5113.

[19] Rivera, J., Garcia, L., Mora, C., Raygoza, J. J. and Ortega, S. Super-Twisting Sliding Mode in Motion Control Systems. In: Bartoszewicz, A. (ed). Sliding Mode Control. Croatia: InTech. 239–254; 2011.

[20] Fischer, N., Hughes, D., Walters, P., Schwartz, E. M. and Dixon, W. E. Nonlinear RISE-Based Control of an Autonomous Underwater Vehicle. IEEE Transactions on Robotics. August 2014. 30(4): 845–852.

[21] Fischer, N., Bhasin, S. and Dixon, W. E. Nonlinear Control of an Autonomous Underwater Vehicle: A RISE-Based Approach. 2011 American Control Conference on O'Farrell Street, San Francisco, CA, USA. June 29–July 01 2011. 3972–3977.

[22] Rhif, A. A High Order Sliding Mode Control with PID Sliding Surface: Simulation on a Torpedo. International Journal of Information Technology, Control and Automation (IJITCA). January 2012. 2(1): 1–13.

[23] Khan, I., Bhatti, A. I., Khan, Q. and Ahmad, Q. Sliding Mode Control of Lateral Dynamics of an AUV. Proceedings of 2012 9th International Bhurban Conference on Applied Sciences & Technology (IBCAST). January 9–12, 2012. Islamabad: IEEE. 27–31.

[24] Li, X., Hou, S. P. and Cheah, C. C. Adaptive Region Tracking Control for Autonomous Underwater Vehicle. Control Automation Robotics & Vision (ICARCV), 2010 11th International Conference. December 7–10, 2010. Singapore: IEEE. 2129–2134.

[25] Ismail, Z. H. and Dunnigan, M. W. Tracking Control Scheme for an Underwater Vehicle-Manipulator System with Single and Multiple Sub-Regions and Sub-Task Objectives. Control Theory & Applications, IET. 2011. 5(5): 721–735.

[26] Li, X. and Cheah, C. C. Adaptive Neural Network Control of Robot Based on a Unified Objective Bound. IEEE Transactions on Control Systems Technology. 2014. 22(3). 1032–1043.

[27] Fossen, T. I. Handbook of Marine Craft Hydrodynamics and Motion Control. First Edition, New York: John Wiley and Sons. 2011.

[28] Ismail, Z. H., Faudzi, A. A. and Dunnigan, M. W. Fault-Tolerant Region-Based Control of an Underwater Vehicle with Kinematically Redundant Thrusters. Mathematical Problems in Engineering. 2014(2014): 1–12. http://dx.doi.org/10.1155/2014/527315

[29] Fridman, L. Chattering Analysis in Sliding Mode Systems with Inertial Sensors. International Journal of Control. 2003. 6(9-10). 906–912.

[30] Fridman, L. and Levant, A. Higher Order Sliding Modes. In: Perruquetti, W. and Barbot, J.-P. (eds). Sliding Mode Control in Engineering. USA: Marcel Dekker, Inc. 53–96; 2002.

[31] Putranti, V., Mokhar, B. and Ismail, Z. H. Sliding Mode Fuzzy Controller for Autonomous Underwater Vehicle under Deterministic Disturbances. Journal of Signal Processing. 2015. 19(4): 143–146.

[32] Salgado-Jimenez, T. and Jouvencel, B. Using a High Order Sliding Modes for Diving Control a Torpedo Autonomous Underwater Vehicle. OCEANS 2003 Proceedings. September 22–26, 2003. San Diego, CA, USA: IEEE. 934–939.

[33] Antonelli, G., Chiaverini, S., Sarkar, N. and West, M. Adaptive Control of an Autonomous Underwater Vehicle: Experimental Results on ODIN. IEEE Transactions on Control Systems Technology. 2001. 9(5): 756–765.

[34] Hong, E. Y., Soon, H. G. and Chitre, M. Depth Control of an Autonomous Underwater Vehicle, STARFISH. OCEANS 2010 IEEE. Sydney, 1–6.